Electron acceleration in the inverse free electron laser with a helical wiggler by axial magnetic field and ion-channel guiding

Reza Khazaeinezhad[1)] Mahdi Esmaeilzadeh

Department of Physics, Iran University of Science and Technology, Tehran, Iran

Abstract: Electron acceleration in the inverse free electron laser (IFEL) with a helical wiggler in the presence of ion-channel guiding and axial magnetic field is investigated in this article. The effects of tapering wiggler amplitude and axial magnetic field are calculated for the electron acceleration. In free electron lasers, electron beams lose energy through radiation while in IFEL electron beams gain energy from the laser. The equation of electron motion and the equation of energy exchange between a single electron and electromagnetic waves are derived and then solved numerically using the fourth order Runge-Kutta method. The tapering effects of a wiggler magnetic field on electron acceleration are investigated and the results show that the electron acceleration increases in the case of a tapered wiggler magnetic field with a proper taper constant.

Key words: IFEL, helical wiggler, ion-channel guiding, axial magnetic field, tapering effects

PACS: 41.75.Jv **DOI:** 10.1088/1674-1137/36/9/015

1 Introduction

One of the great challenges in the field of accelerating particles by laser radiation is producing an electron beam with bunch length which is smaller than half laser wavelength; however it is important for efficient acceleration and to get small energy spread. Several techniques are proposed for producing a micro-bunch electron beam in applications of acceleration [1, 2].

Due to the high energy of electrons used in several fields, such as fusion and X-ray generation [3, 4], accelerating electron beams by laser waves is one of the research areas in progress [5].

The inverse free electron laser, as can be inferred from its name, works inversely in the resonance mode of free electron laser. In the resonance mode of free electron laser, the first laser pulse is sent into the helical field along with the electron beam; if the direction of electron wiggling motion is against the electric field of laser pulse, the energy is transferred from waves to electrons, and consequently, electrons are accelerated. In the case that electric field and electron velocity are in the same direction, the kinetic energy of electrons is transferred to waves and waves are enhanced.

The inverse free electron laser (IFEL) resonance condition is $\lambda/\lambda_{\rm w} = 1/(1/V_z - 1)$; λ, $\lambda_{\rm w}$ and V_z are electron's wavelength, wiggler's wavelength and electron velocity respectively; that depends on the electron energy and the electron density of the medium. Tapering and chirping are two methods for satisfying the resonance condition. The tapering method is used in many articles such as Ref. [6].

Also in this paper the tapering method is used for satisfying the resonance condition as well as increasing the electron energy gained.

Using inverse free electron laser as a device for accelerating and micro-bunching has several advantages. Since the inverse free electron lasers do not use any material environment, it has no problems such as unstable plasma and dispersion of the nonlinear laser pulse.

In the 1970s [7], the inverse free electron lasers were first described for high-gradient particle accelerators [8]. Experimental results show that the inverse free electron lasers accelerate electrons and in addi-

Received 15 November 2011

1) E-mail: reza.kh.n@gmail.com

tion are capable of producing micro-bunch [9], phase-dependent acceleration of electrons [10], phase locking and multi-stage acceleration [11] and control of final energy spread [12]. The study of IFEL as a potential mode of electron acceleration was pursued at Brookhaven National Laboratory (BNL) in 1992 [13]. The experiment used a 50 MeV electron beam, a 15 GW CO_2 laser beam provided by the BNLs Accelerator Test Facility and a uniquely designed period length tapered wiggler [14]. In 2004, the IFEL experimented at the Neptune laboratory at the University of California accelerated the electrons from 14.5 MeV up to more than 35 MeV utilizing a CO_2 laser beam with a peak power (0.4 TW), one order of magnitude greater than any other previous IFEL experiments had used [15].

In recent years, a variety of investigations have been researched [6, 16]. But in these inquiries a helical magnetic field with both an axial magnetic field and ion-channel guiding has not been used.

The wiggler magnetic field is the periodic static magnetic field, which has an essential role in increasing the laser gain. A uniform static axial magnetic field is often employed to guide the propagation of the electron beam through the wiggler, and to enhance the gain. As an alternative to guiding the relativistic electron beam by using an axial magnetic field and ion-channel guiding is proposed in Ref. [17]. This technique involves the creation of a plasma channel by passage of a UV-laser beam through a gas. The plasma electrons are then electro-statically repelled by the injection of a relativistic electron beam through the channel. The resulting ion-channel attracts and transversely confines the beam electrons.

In this paper, electron acceleration in the IFEL with a helical wiggler in the presence of ion-channel guiding and axial magnetic field has been studied. This paper is organized as follows: the helical wiggler is described briefly in the following section. In Section 3, relativistic equations for electron motion are presented. Simulation results are shown in Section 4. Finally, the conclusions are drawn in Section 5.

2 Helical wiggler

The helical wiggler magnetic field is generated by helical winding of two wires on the cylinder, with a current flow in opposite direction. That is shown in Fig. 1.

The wiggler magnetic field is considered in two states, real and ideal. The real state is a derivation

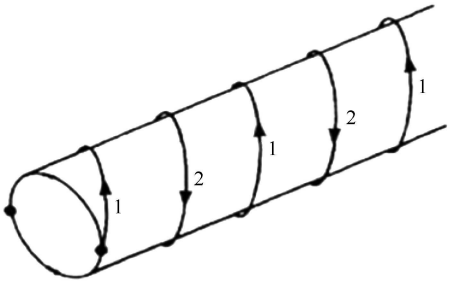

Fig. 1. The winding cylindrical for generated helical magnetic field.

of Maxwell equations without any approximation. That is a complex function of Bessel functions. Eq. (1) shows the real state in the cylindrical coordinate system [18, 19]:

$$\boldsymbol{B}_{\rm w} = 2B_{0d}\left[I_1'(\lambda)\cos\chi\hat{e}_r - \frac{1}{\lambda}I_1(\lambda)\sin\chi\hat{e}_\theta + I_1(\lambda)\sin\chi\hat{e}_z\right], \tag{1}$$

where B_{0d} is the amplitude of the wiggler magnetic field and,

$$\lambda = k_{\rm w}r, \tag{2}$$

$$\chi = \theta - k_{\rm w}z, \tag{3}$$

$$k_{\rm w} = \frac{2\pi}{\lambda_{\rm w}}, \tag{4}$$

where $k_{\rm w}$ and $\lambda_{\rm w}$ are the wiggler's wave vector and the wiggler's wavelength, respectively. Real state in Cartesian coordinate system is:

$$B_{{\rm w}x} = 2B_{0d}\left[\frac{1}{2}(I_0(\lambda)+I_2(\lambda))\cos\chi\cos\theta - \frac{1}{\lambda}I_1(\lambda)\sin\chi\sin\theta\right], \tag{5}$$

$$B_{{\rm w}y} = 2B_{0d}\left[\frac{1}{2}(I_0(\lambda)+I_2(\lambda))\cos\chi\sin\theta - \frac{1}{\lambda}I_1(\lambda)\sin\chi\cos\theta\right], \tag{6}$$

$$B_{{\rm w}z} = -2B_{0d}I_1(\lambda)\sin\chi. \tag{7}$$

The ideal state is a simplified real state with approximation for $\lambda \ll 1$ that is returned in Eq. (8):

$$\boldsymbol{B}_{\rm w} = B_{0d}[\cos(k_{\rm w}z)\hat{e}_x + \sin(k_{\rm w}z)\hat{e}_y]. \tag{8}$$

3 Relativistic analysis

In this section, equations of electron motion with helical wiggler, ion-channel guiding and axial magnetic field are derived. Considering the propagation of a laser pulse with a vector potential,

$$A = A_0 [\hat{x}\cos(\omega t - kz) + \hat{y}\sin(\omega t - kz)] \times \exp\left[-[t-(z-z_1)/v_g]^2/t_1^2\right], \quad (9)$$

where, A_0 and z_1 are the amplitude of vector potential and the initial position of the pulse peak, respectively. Also, v_g is the group velocity with the following equation [6]:

$$v_g = c\left(1-\omega_p^2/\omega^2\right)^{1/2}, \quad (10)$$

and

$$k = (\omega/c)\times\left(1-\omega_p^2/\omega^2\right)^{1/2}, \quad (11)$$

that

$$\omega_p^2 = e^2 n_b/m\varepsilon_0, \quad (12)$$

where ω_p, $-e$, n_b and m are the relativistic plasma frequency, electron charge, density of beam electrons and effective mass, respectively.

An electrostatic field is generated by the ion-channel with positive charge $+e$ and density n_i, which can be written as follows:

$$\boldsymbol{E}_u = \frac{e^2 n_i}{2\varepsilon_0}(x\hat{e}_x + y\hat{e}_y). \quad (13)$$

Also, the axial magnetic fields along with axial laser are:

$$\boldsymbol{B} = B_0\hat{e}_z, \quad (14)$$

B_0 is the initial axial magnetic field. When the electron beam enters into the wiggler it has a direct movement and its velocity is along the wiggler axial. The wiggler magnetic field causes the electron beam to bend along the width axial; therefore, partial advance velocity is decreased and changed to a width velocity. By gradually declining the intensity of the axial magnetic field or period of the wiggler magnetic field, the electrons' width velocity are changed into axial velocity.

So, consider the axial magnetic field as Eq. (14)

$$\begin{cases} B = B_0\left(\dfrac{z}{z_0}\right)\hat{e}_z - \dfrac{B_0}{2z_0}(x\hat{e}_x + y\hat{e}_y) & \text{for } z \leqslant z_0 \\ B = B_0\,\hat{e}_z & \text{for } z > z_0 \end{cases} \quad (15)$$

where, z_0 is the initial state.

Also, for the period of the wiggler magnetic field,

$$\begin{cases} B_w = B_{w0}\sin^2\left(k_w\left(\dfrac{z}{4N}\right)\right) & \text{for } z \leqslant N\lambda_w \\ B_w = B_{w0} & \text{for } z > N\lambda_w \end{cases} \quad (16)$$

$$\lambda_w = \frac{2\pi}{k_w}, \quad (17)$$

B_{w0} and k_w are the periodical wiggler magnetic field and wave vector, respectively.

So, we can use a tapered axial magnetic field, a tapered periodical wiggler magnetic field, or both of them; therefore, equation of the energy exchange rate between electron and wave is:

$$\frac{d\gamma}{dt} = -\frac{e}{m_0c^2}v.E. \quad (18)$$

The electromagnetic fields related to the vector potential of the laser pulse are

$$E = -\frac{\partial A}{\partial t}, \quad (19)$$

$$B = \nabla\times A. \quad (20)$$

The Lorentz force is:

$$\frac{dP}{dt} = -e(E + v\times B). \quad (21)$$

Eventually the equations of electron motion are obtained as follows:

$$\frac{dP_x}{dt} = e\frac{\partial A_x}{\partial t} + ev_z\left(\frac{\partial A_x}{\partial z} + B_{wy}\right) - ev_yB_0 - \left(\frac{\pi e^2}{2\varepsilon_0}n_i\right)x, \quad (22)$$

$$\frac{dP_y}{dt} = e\frac{\partial A_y}{\partial t} + ev_z\left(\frac{\partial A_y}{\partial z} + B_{wx}\right) + ev_x(B_0 + B_{wz}) - \left(\frac{\pi e^2}{2\varepsilon_0}n_i\right)y, \quad (23)$$

$$\frac{dP_z}{dt} = -ev_x\left(\frac{\partial A_x}{\partial z} + B_{wy}\right) - ev_y\left(\frac{\partial A_y}{\partial z} + B_{wx}\right). \quad (24)$$

The equation governing the energy exchange rate between electron and wave is:

$$\frac{d(\gamma m_0c^2)}{dt} = ev_x\frac{\partial A_x}{\partial t} + ev_y\frac{\partial A_y}{\partial t} - \left(\frac{\pi e^2}{2\varepsilon_0}n_i\right)(xv_x + yv_y). \quad (25)$$

In the following discussion we will use the dimen-

sionless variables

$$\begin{cases} a_0 \to \dfrac{eA_0}{m_0 c},\ b_0 \to \dfrac{eB_0}{m_0\omega},\ t \to \omega t,\ t_1 \to \omega t_1, \\ x \to \omega x/c,\ y \to \omega y/c,\ z \to \omega z/c, \\ z_1 \to \omega z_1/c,\ k \to kc/\omega, \\ \vec{V} \to \dfrac{\vec{v}}{c},\ P_{x0} \to P_{x0}/m_0 c, \\ P_{y0} \to P_{y0}/m_0 c,\ P_{z0} \to P_{z0}/m_0 c, \\ \mathrm{d}x/\mathrm{d}t \to (k/\omega)\,\mathrm{d}x/\mathrm{d}t, \\ \mathrm{d}y/\mathrm{d}t \to (k/\omega)\,\mathrm{d}y/\mathrm{d}t, \\ \mathrm{d}z/\mathrm{d}t \to (k/\omega)\,\mathrm{d}z/\mathrm{d}t, \\ \lambda_{\mathrm{L}}/\lambda_{\mathrm{w}} \to k_{\mathrm{w}}/k, \end{cases} \tag{26}$$

Substituting Eq. (26) into Eqs. (22), (23), (24) and (25) leads to:

$$\frac{\mathrm{d}V_x}{\mathrm{d}t} = \frac{1}{\gamma}\left(\frac{\partial A_x}{\partial t} + V_z\left(\frac{\partial A_x}{\partial z} + B_{\mathrm{w}y}\right) - V_y(B_0 + B_{\mathrm{w}z})\right) - \frac{1}{\gamma}\omega_i^2 x - \frac{1}{\gamma}\frac{\mathrm{d}\gamma}{\mathrm{d}t}V_x, \tag{27}$$

$$\frac{\mathrm{d}V_y}{\mathrm{d}t} = \frac{1}{\gamma}\left(\frac{\partial A_y}{\partial t} + V_z\left(\frac{\partial A_y}{\partial z} + B_{\mathrm{w}x}\right) + V_x(B_0 + B_{\mathrm{w}z}) - \frac{1}{\gamma}\omega_i^2 y - \frac{1}{\gamma}\frac{\mathrm{d}\gamma}{\mathrm{d}t}V_y, \tag{28}$$

$$\frac{\mathrm{d}V_z}{\mathrm{d}t} = -\frac{1}{\gamma}(V_x\left(\frac{\partial A_x}{\partial z} + B_{\mathrm{w}y}\right) + V_y\left(\frac{\partial A_y}{\partial z} + B_{\mathrm{w}x}\right) - \frac{1}{\gamma}\frac{\mathrm{d}\gamma}{\mathrm{d}t}V_z, \tag{29}$$

$$\frac{\mathrm{d}\gamma}{\mathrm{d}t} = \left(V_x\frac{\partial A_x}{\partial t} + \upsilon_y\frac{\partial A_y}{\partial t}\right) - \omega_i^2(xV_x + yV_y). \tag{30}$$

Equations (27)–(30) are the equations of electron motion with a helical wiggler, ion-channel guiding and axial magnetic field.

4 Simulation result

Equations (27)–(30) and $V_x = \dfrac{\mathrm{d}x}{\mathrm{d}t}$, $V_y = \dfrac{\mathrm{d}y}{\mathrm{d}t}$, $V_z = \dfrac{\mathrm{d}z}{\mathrm{d}t}$ are seven coupled equations that are solved numerically with MATLAB programming using the fourth order Runge-Kutta method. Electron trajectories in three-dimensional space and energy γ, as a function of z for different conditions of magnetic field, have been obtained. The results are illustrated in the state of dimensionless variables. Parameters are optimized for satisfying the resonance condition; as a result, energy gained by the electron increases. Optimal parameters have been chosen for this inquiry:

$a_0 = 20,\ k = 0.999,\ z_1 = -100,\ \tau_1 = 50,$

$\omega_i = 0.01,\ B_0 = 0.1,\ B_{\mathrm{w}0} = 0.09,\ k_{\mathrm{w}} = 0.001,$

The initial electron energy is considered $\gamma_0 = 2.78$ in all sections for comparison of increasing acceleration.

Figure 2 shows the electron trajectory in three-dimensional space by helical wiggler, ion-channel guiding and axial magnetic field. Apparently, electron trajectory does not have fixed motion in the initial time, but reaching the final acceleration in the presence of the wiggler, continues its motion in a stable trace. Fig. 3 demonstrates the electron energy γ as a function of z by the ideal state of the helical wiggler and axial magnetic field. Fig. 4 depicts the electron energy γ as a function of z by the real state of the helical wiggler and axial magnetic field. In these cases, since we do not use ion-channel guiding in equation of motions, we set $\omega_i = 0$. Also, it shows tapering effects in these figures; however if tapering effects are considered in periodical wiggler magnetic field and axial magnetic field, more gain is obtained

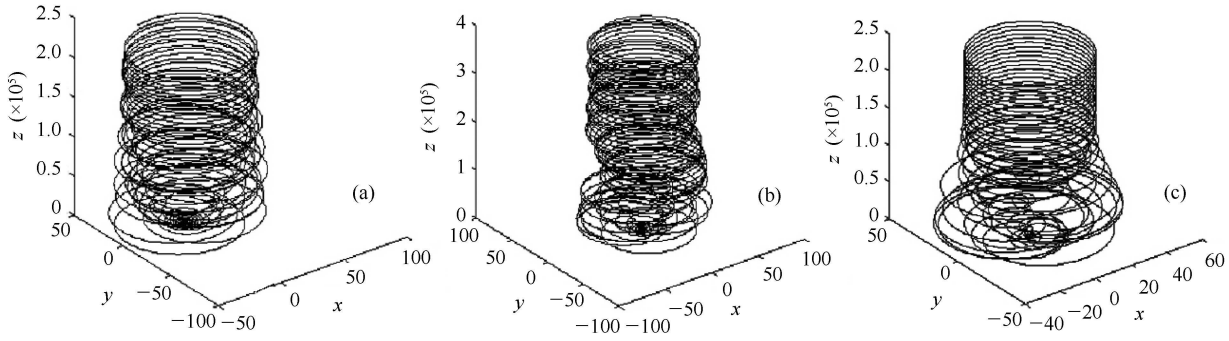

Fig. 2. (a) Electron trajectory in 3-D space by a helical wiggler and axial magnetic field; (b) Electron trajectory in 3-D space by a helical wiggler and ion-channel guiding; (c) Electron trajectory in 3-D space by a helical wiggler, axial magnetic field and ion-channel guiding.

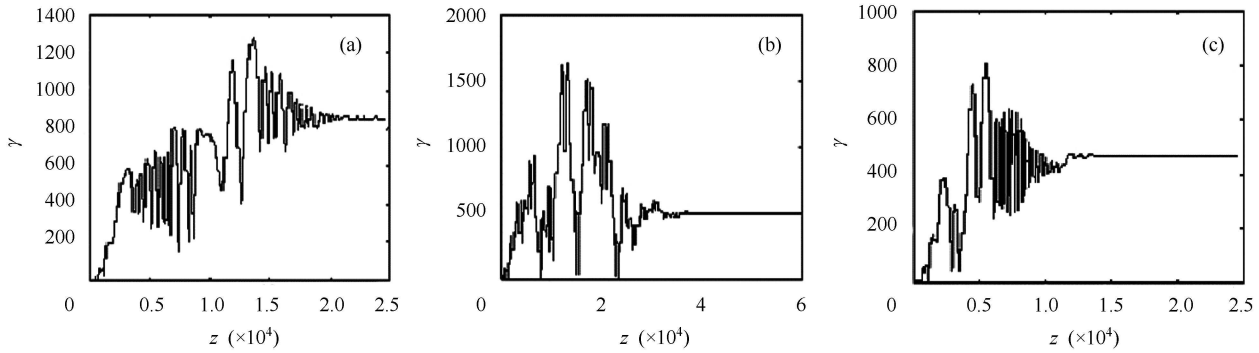

Fig. 3. (a) The electron energy as a function of z by ideal state of tapered helical wiggler and tapered axial magnetic field; (b) The electron energy as a function of z by ideal state of a helical wiggler and tapered axial magnetic field; (c) The electron energy as a function of z by ideal state of a tapered helical wiggler and axial magnetic field.

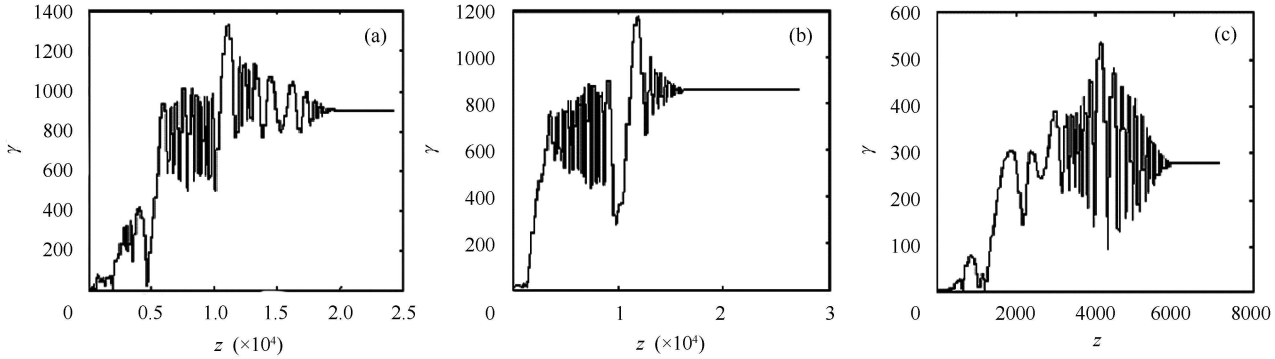

Fig. 4. (a) The electron energy as a function of z by real state of a tapered helical wiggler and tapered axial magnetic field; (b) The electron energy as a function of z by real state of a helical wiggler and tapered axial magnetic field; (c) The electron energy as a function of z by real state of a tapered helical wiggler and axial magnetic field.

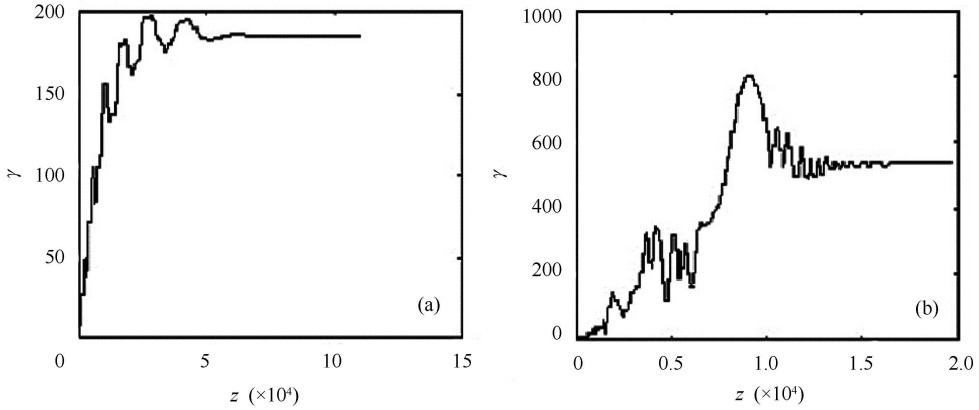

Fig. 5. (a) The electron energy γ as a function of z by ideal state of a tapered helical wiggler; (b) The electron energy γ as a function of z by real state of a helical wiggler.

in comparison with the time that one of them is tapered.

Figures 5 demonstrates the electron energy γ by the ideal and real states of the helical wiggler and ion-channel guiding. Because of no axial magnetic field, $B_0 = 0$. Comparison of (3)–(5) figures shows that the electron is accelerated more in the presence of the axial magnetic field in contrast with the time that ion-channel guiding is used.

Electron energy γ with the helical wiggler in the presence of ion-channel guiding and axial magnetic field is illustrated in Figs. 6 and 7. Again in cases,

when tapering effects are considered in the periodical wiggler magnetic field, the axial magnetic field is likely to gain the most. As well as in Fig. 6(a) it is observed that maximum acceleration of electrons is obtained by ion-channel guiding and axial magnetic field. Also in a realistic helical wiggler, the electron gains energy more than that in an idealized helical wiggler.

Approximate electron energy γ by ion-channel guiding and axial magnetic field is written in Table 1.

If these results are compared with the previous research in this field, such as Ref. [16] in which the acceleration of electrons is studied just in the presence of axial magnetic field and Ref. [6] which investigates just the tapering effect, we can perceive that not only do these results confirm previous work, but also the electron is much more accelerated, because of using the helical wiggler and ion-channel guiding and tapering effect.

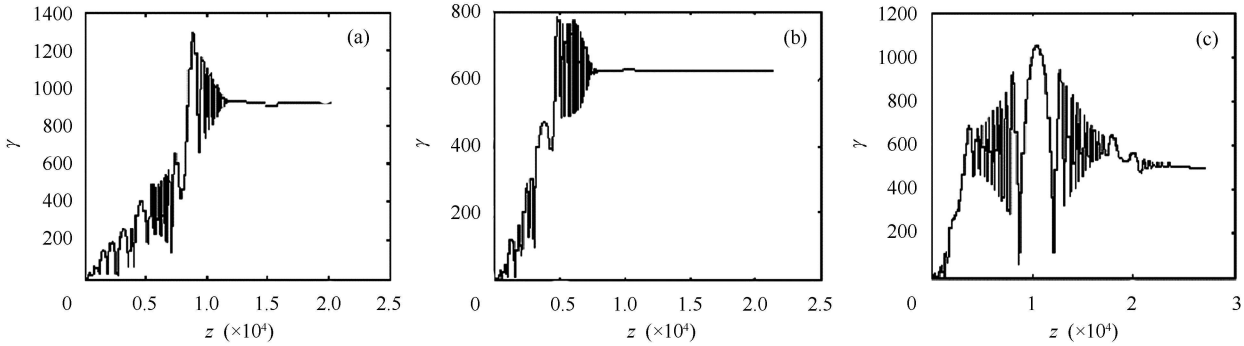

Fig. 6. (a) The electron energy γ as a function of z by the ideal state of the tapered helical wiggler, tapered axial magnetic field and ion-channel guiding; (b) The electron energy γ as a function of z by the ideal state of the helical wiggler, tapered axial magnetic field and ion-channel guiding; (c) The electron energy γ as a function of z by the ideal state of the tapered helical wiggler, axial magnetic field and ion-channel guiding.

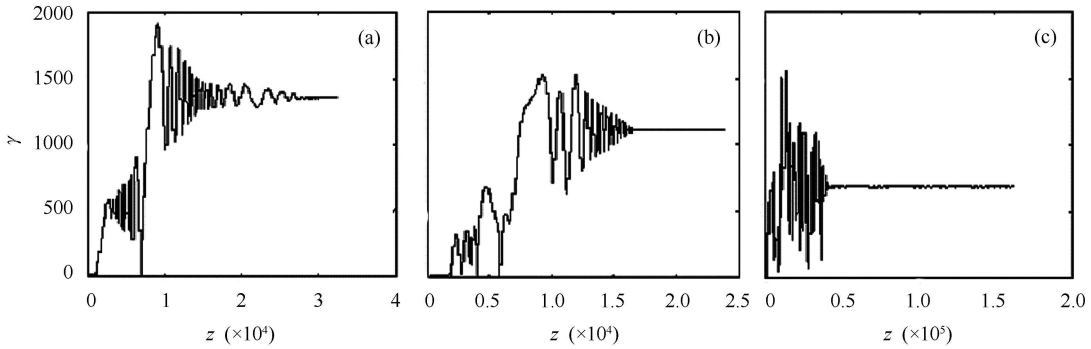

Fig. 7. (a) The electron energy γ as a function of z by real state of tapered helical wiggler, tapered axial magnetic field and ion-channel guiding; (b) The electron energy γ as a function of z by real state of helical wiggler, tapered axial magnetic field and ion-channel guiding; (c) The electron energy γ as a function of z by real state of a tapered helical wiggler, axial magnetic field and ion-channel guiding.

Table 1. Approximate electron energy γ by ion-channel guiding and axial magnetic field.

	without ion-channel guiding			with ion-channel guiding			
	tapered helical wiggler and tapered axial magnetic field	helical wiggler and tapered axial magnetic field	tapered helical wiggler and axial magnetic field	tapered helical wiggler	tapered helical wiggler and tapered axial magnetic field	helical wiggler and tapered axial magnetic field	tapered helical wiggler and axial field
ideal helical wiggler	820	500	430	180	900	600	500
real helical wiggler	900	850	300	500	1400	1100	700

5 Conclusion

In this paper, the acceleration of electrons in the inverse free electron lasers has been studied with the helical wiggler in the presence of ion-channel guiding and axial magnetic field. For this purpose, the electron equation of motion and the equation of energy exchange between a single electron and electromagnetic wave are numerically solved using the fourth order Runge-Kutta method.

The ion-channel guiding and axial magnetic field prevent the spreading of the electron beam in the direction of electron beam emissions which are added to the system. According to the results, the axial magnetic field is more useful and better than the ion-channel guiding, and, because more energy is achieved by the presence of the axial magnetic field, it prevents electron diffusion more than ion-channel guiding. By gradually declining the intensity of the axial magnetic field or period of the wiggler magnetic field, so called tapering effects, better electron acceleration is achieved. When the tapering effects are considered in the periodical wiggler magnetic field and axial magnetic field, more gain is obtained than when one of them is tapered.

Finally, electrons attain maximum acceleration with the real state of the tapered helical wiggler in the presence of ion-channel guiding and tapered axial magnetic field.

References

1 Serafini L. IEEE Trans. on Plasma Science, 1996, **42**: 421
2 Katsouleas T C, Clayton C E, Serafini L et al. IEEE Trans. on Plasma Science, 1996, **24**: 443
3 Ren C, Tzoufras M, Tonge J et al. Phys. Plasmas, 2006, **13**: 056308
4 Fritzler S, Ta Phuoc K, Malka V et al. Appl. Phys. Letts., 2003, **83**: 3888
5 Hafz N, Lee H J, Kim J U et al. IEEE Trans. on Plasma Science, 2003, **31**: 1388
6 Singh K P, Tripathi V K . Physics of Plasmas, 2004, **11**: 743
7 Palmer R. Journal of Applied Physics, 1972, **43**: 3014
8 Courant K, Pellegrini C, Zakowicz W. Phys. Rev. A, 1985, **32**: 2813
9 LIU Y, WANG X J, Cline D B et al. Physical Review Letters, 1998, **80**: 4418
10 Yolder R B, Marshall T C, Hirshfield J L. Physical Review Letters, 2000, **86**: 1765
11 Kimura W D, Steenbergen A V, Babzien M et al. Physical Review Letters, 2001, **86**: 4041
12 Kimura W D, Babzien M, Ben-Zvi I et al. Physical Review Letters, 2004, **92**: 054801
13 Wernick I, Marshall T C. Phys. Rev. A, 1992, **46**: 3566
14 Steenbergen A V, Gallardo J, Sandweiss J et al. Physical Review Letters, 1996, **77**: 2690
15 Musumeci P, Tochitsky S Y, Boucher S et al. American Institute of Physics, 2004, **737**: 160
16 Singh K P, Physics of Plasma, 2004, **11**: 3992
17 Jha P, Kumar P. IEEE Trans. Plasma Sci., 1996, **24**: 1359
18 Esmaeilzadeh M, Ebrahimi S, Saiahian A et al. Physics of Plasmas, 2005, **12**: 093103
19 Esmaeilzadeh M, Fallah M S, Willett J E. Physics of Plasmas, 2007, **14**: 013103